Projectile excitation to autoionizing states in swift collisions of open-shell He-like ions with helium

A. Laoutaris,[1,2] S. Nanos,[2,3,*] A. Biniskos,[3,†] S. Passalidis,[4,‡] E. P. Benis,[3] A. Dubois,[4,§] and T. J. M. Zouros[1,‖]

[1]*Department of Physics, University of Crete, GR-70013 Heraklion, Greece*

[2]*Tandem Accelerator Laboratory, Institute of Nuclear and Particle Physics, NCSR "Demokritos", GR-15310 Ag. Paraskevi, Greece*

[3]*Department of Physics, University of Ioannina, GR-45110 Ioannina, Greece*

[4]*Sorbonne Université, CNRS, Laboratoire de Chimie Physique- Matière et Rayonnement, F-75005 Paris, France*

(Received 29 December 2023; accepted 21 February 2024; published 29 March 2024)

Atomic orbital close-coupling calculations involving three active electrons within a full configuration interaction formalism are used to investigate projectile excitation. Cross sections for the production of the autoionizing $(2s2p\ ^3P)$ states in 0.5–1.5 MeV/u collisions of $C^{4+}(1s2s\ ^3S)$ and $O^{6+}(1s2s\ ^3S)$ ions with He are presented. Results are compared to accompanying 0° Auger projectile spectroscopy measurements. While the projectile energy dependence of the theoretical results is in overall agreement with experiment, theory is found to be somewhat smaller than experiment. Critical comparisons to first-order Born and a minimal basis close-coupling calculation indicate that the use of low-order perturbative treatments and related interpretations may be questionable in this energy range. Such a nonperturbative treatment, which does not rely on any scaling parameters or renormalization, is seen to provide an important advance in the modeling of multielectron multi-open-shell quantum systems under ultrafast perturbations, whose understanding seems to still be incomplete.

DOI: 10.1103/PhysRevA.109.032825

I. INTRODUCTION

The excitation of an electron from one bound state to another in an atom or ion is a fundamental quantum mechanical process pervading most atomic physics. Together with electron capture and ionization, it constitutes one of the most important ion-atom collision processes. Apart from its interest to atomic physics, such excitations are responsible for the vast majority of x-ray radiation encountered in various kinds of plasmas in astrophysics [1], in high-energy density physics experiments, and in laboratory fusion devices [2,3]. Thus, it is surprising that such excitation processes in atomic collisions have received much less attention either theoretically or experimentally than electron capture or ionization, particularly since there remain substantial differences between theory and experiment even for the most basic collision systems, such as $H(1s) + H(1s)$ and $He^+(1s) + H(1s)$ (see Refs. [4,5] and references therein).

While the excitation of H and He by particle beams such as electrons (see, for example, [6,7] and references therein) or bare ions [8–10] has reached a high level of sophistication and accuracy utilizing *ab initio* nonperturbative treatments also, excitation with ions carrying electrons into the collision (known as *dressed* ions) is not yet as advanced, mostly relying on perturbative treatments. The additional projectile electrons introduce considerable complexity, acting not only as passive screening agents, but also as dynamic exciting agents themselves, clearly demonstrating phenomena such as collision energy thresholds and electron exchange interactions [11]. Furthermore, in most experiments, the final state of the target following projectile excitation is not usually determined. Therefore, contributions from both ground- and excited-target states (including ionization) need to be considered for an accurate comparison to experiment, further increasing the difficulty of the calculations.

In dressed ion-atom collisions, such an excitation is realized through the Coulomb interaction of the excited electron with either (a) the positively charged (screened) nucleus via electron-nucleus $(e - n)$ interactions or (b) the electrons via electron-electron $(e - e)$ interactions of the colliding partners (see reviews [11–16] and references therein, as well as [17] for relativistic collisions). Investigations have focused mostly on the excitation of highly charged few-electron *projectiles* in collisions with simple targets such as H and He to make the problem more tractable.

Experimentally, such excitations have been investigated using ion beams provided by accelerators, where the impact energy E_p and the atomic number of the projectile ion, Z_p, can be varied. Thus, *projectile* excitation has been investigated with the additional advantage that the projectile charge state q (and therefore the number of electrons carried into the collision, $Z_p - q$) can also be controlled, allowing for invaluable isoelectronic projectile excitation studies as a function of both E_p and Z_p for different initial ground-state configurations of the projectile. In particular, *state-selective* projectile excitation has been investigated primarily through the high-resolution recording of the emitted ensuing photon [18–22]

*Present address: Department of Physics, University of Crete, GR-70013 Heraklion, Greece.

†Present address: Institut für Kernphysik, J. W. Goethe-Universität Frankfurt am Main, 60438 Frankfurt am Main, Germany.

‡Present address: CEA, DAM, DIF, 91297 Arpajon, France and Université Paris-Saclay, CEA, LMCE, 91680 Bruyères-le-Châtel, France.

§alain.dubois@sorbonne-universite.fr

‖tzouros@physics.uoc.gr

or Auger electron [23–28] for various collision systems, including even relativistic H-like [29] or He-like uranium [30]. More recently, the possibility to also use initial projectile configurations other than the ground state, such as the $1s2s\ ^3S$ excited metastable state in He-like ions, opens up new excitation channels such as the production of doubly excited states, thus becoming amenable to high-resolution Auger spectroscopy even for He-like systems.

Theoretically, early investigations predominantly used *first-order perturbation* theory based primarily on the plane-wave Born approximation (PWBA) [31] to calculate $1s \rightarrow nl$ target excitation of H or He, first by *bare* projectiles including protons and heavier ions, but also of *dressed* projectiles [32] in the framework of an independent electron approximation establishing useful semiempirical scaling law dependencies on q and Z_p and an overall understanding of target excitation [20]. However, with the advent of growing computer power, *nonperturbative* close-coupling calculations (see [33] and references therein) more and more took over effectively as the state of the art using one, two [34,35], or even three [36] active electrons with increasingly larger basis states to describe excitation, single-electron capture (SEC), transfer-excitation (TE), and target ionization (TI). Of course, for fast enough collisions, cross sections for the excitation of both perturbative and nonperturbative approaches should converge, thus providing ways to check theoretical results and establish common validity regions.

In this paper, we provide a comprehensive investigation of projectile excitation combining close-coupling calculations for *three* active electrons with state-selective single-differential cross-section ($d\sigma/d\Omega'$) Auger electron measurements. Here, we focus on the production of the $2s2p\ ^3P$ state (for short, ^3P), which is excited from the $1s2s\ ^3S$ (for short, ^3S) initial state of the X^{q+} ion-beam component,

$$X^{q+}(^3S) + \mathrm{He} \rightarrow X^{q+}(^3P) + \mathrm{He(All)} \quad \text{(excitation)}, \tag{1}$$

$$\hookrightarrow X^{(q+1)+}(1s) + e_A^-(0^\circ)\ \text{(Auger)}, \tag{2}$$

where X^{q+} stands for C^{4+} or O^{6+} ion projectiles, and the Auger electron e_A^- in process (2) is detected at the $\theta = 0^\circ$ laboratory observation angle with respect to the ion beam. Contributions from various final target states following projectile excitation [symbolized by He(All), i.e., He in the ground, excited, or ionized states] are also considered since, in the experiment, the final state of the target is not determined. A critical discussion with results obtained using the long-established first-order Born approximation, as well as an additional *minimal-basis* close-coupling calculation, is also included.

II. EXPERIMENT

Our measurements were conducted at the National Center for Scientific Research (NCSR) "Demokritos" 5.5 MV Tandem accelerator facility [37]. He-like carbon and oxygen ions were accelerated to 0.5–1.5 MeV/u with about 0.2–20 nA beam intensities on target depending on energy and stripping conditions. The initially negative ion beams were produced either by a sputter (for C^-) or duoplasmatron (for O^-) ion source and were stripped once in the tandem accelerator terminal. Below about 1 MeV/u for carbon and, for most of the collision energies, for oxygen, a second stripping after the analyzer magnet (poststripping) was required to obtain sufficient beam intensities. The stripping systems utilized thin self-supporting carbon foils or N_2 gas.

In the experiment, the He-like ions are naturally delivered from the accelerator in a mixture of ground-state ($1s^2$) and metastable-state ($1s2s\ ^{1,3}S$) components. Due to the long lifetime of the $1s2s\ ^3S$ states, they survive to the target and are mixed in with the ground-state ions [38]. The number of ions in the metastable state is controlled by varying the density of the stripping medium [39]. The $2s2p\ ^3P$ state is found to be predominantly produced by direct excitation from the ($1s2s\ ^3S$) state, while contributions from the ground-state or ($1s2s\ ^1S$) beam components can be considered negligible since they involve much lower probability processes such as double excitation or single excitation with spin exchange, respectively. In addition, the amount of ($1s2s\ ^1S$) component surviving to the target is less than a few percent due to its much shorter lifetime [38].

The technique of 0° Auger projectile spectroscopy (ZAPS) [40] is used to record the emitted Auger electrons e_A^- at $\theta = 0^\circ$ with respect to the beam direction [see Eq. (2)]. The metastable fraction $f[^3S]$, which critically depends on the stripping parameters, is also experimentally determined *in situ* from the same spectrum [39]. Finally, excitation of such strongly autoionizing states of low-Z_p ions is relatively free from cascade complications associated with similar x-ray spectroscopy of singly excited states (see Sec. IV B). Overall, the above conditions contribute to a rather clean and well-controlled experimental environment.

Our ZAPS setup is centered around a hemispherical electron spectrograph with a preretardation lens and a doubly differentially pumped target gas cell, as already described [41–43]. To attain sufficient energy resolution, the analyzed Auger electrons were preretarded in the injection lens of the hemispherical analyzer by a factor of 4. The spectrograph transmission is determined by three electroformed meshes of 90% transmission each. The absolute overall spectrograph efficiency η was obtained by performing auxiliary *in situ* measurements of either elastically scattered (binary encounter) electrons from bare C^{6+} ion beams, as typically done for increased accuracy in all such ZAPS measurements [40], and/or measurements of target Ne-*KLL* Auger production utilizing proton beams [44]. Both methods gave very similar results, i.e., an overall efficiency $\eta = (50 \pm 5)\%$. In addition, our present data acquisition system allows for a maximum count rate of about 100 kHz with negligible dead time. The above parameters were carefully determined in a concerted effort to obtain accurate absolute cross sections. Typical spectra normalized to the total number of ions (also known as double differential cross sections or DDCS) in the mixed-state beam are shown in Fig. 1.

Both $2s2p\ ^3P$ and $2s2p\ ^1P$ excitation lines are clearly seen to lie a bit higher in electron energy than the well-known $1s2l2l'\ KLL$ Auger lines produced by SEC [36,42] or TE [43]. Normalized $\theta = 0^\circ$ Auger electron yields, $dY_A^{\mathrm{exp}}(0^\circ)/d\Omega'$, were extracted by peak fitting the Auger lines of interest. Absolute Auger single-differential cross sections (SDCSs) for the production of $2s2p\ ^3P$ were then obtained from the Auger

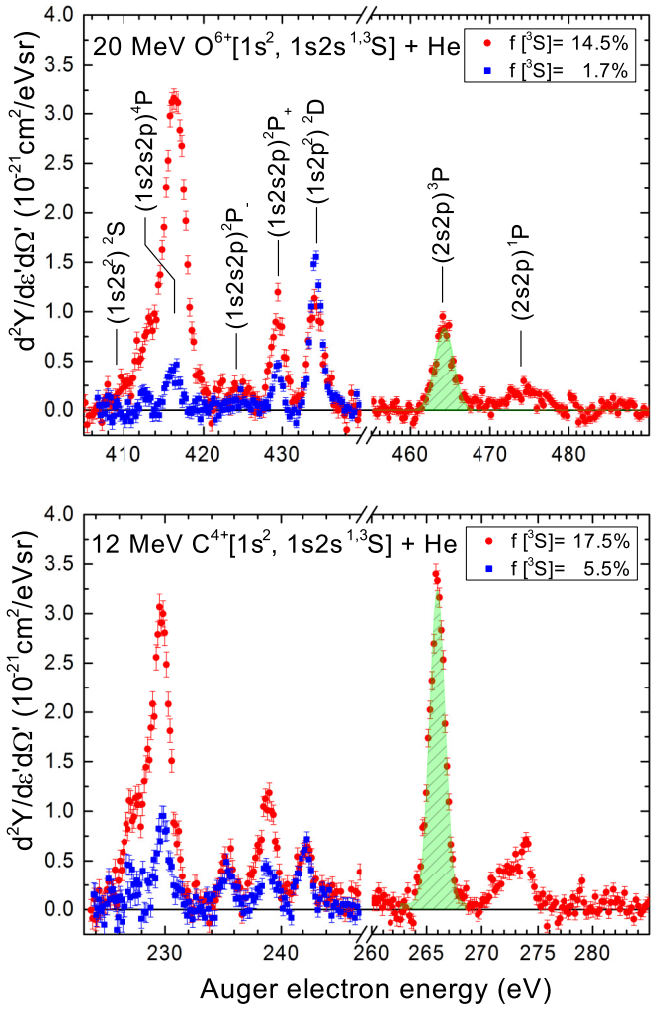

FIG. 1. Example of normalized Auger electron yields measured at $\theta = 0^\circ$ with respect to the projectile for 12 MeV C^{4+} (bottom) and 20 MeV O^{6+} (top) mixed-state beams in collision with He, after transformation to the rest frame of the projectile (primed quantities). Right: The $2s2p\ ^3P$ Auger line, investigated here, produced by excitation from the $1s2s\ ^3S$ component of the ion beams is highlighted (green shading). Left: Auxiliary Auger *KLL* spectra produced in the same collisions are used in the determination of the $1s2s\ ^3S$ metastable fraction $f[^3S]$. Both high (red) and low (blue) metastable fraction spectra are indicated.

yields as

$$\frac{d\sigma_A^{\rm exp}}{d\Omega'}(0^\circ) = \frac{1}{f[^3S]}\frac{dY_A^{\rm exp}}{d\Omega'}(0^\circ). \tag{3}$$

The $f[^3S]$ fraction was determined experimentally from the Li-like *KLL* Auger spectrum also accumulated within the same measurement using our "two-spectra" measuring technique, as described in detail in previous publications [39,41,45]. The $2s2p\ ^3P$ SDCSs, shown in Fig. 3, were determined according to Eq. (3) from the high metastable fraction spectra for improved statistics.

III. THEORY

In this section, we present our theoretical results obtained using the atomic orbital close-coupling approach with three active electrons referred to as 3eAOCC in the following. In addition, for the sake of completeness, we also present total cross sections for excitation using the PWBA from which most of our present understanding of excitation in ion-atom collisions derives. Finally, to compare with our experimental SDCS determined at the observation angle $\theta = 0^\circ$, we also present the necessary theoretical Auger angular distribution formulas.

A. Three-electron atomic orbital close coupling

A semiclassical close-coupling approach was employed for both carbon and oxygen projectiles to describe the excitation process in Eq. (1). The treatment is based on a time-dependent expansion of the scattering states onto sets of asymptotic states, i.e., states of the two isolated target and projectile partners of the collision, with exact antisymmetrization of the three-electron, two-center total wave function. Furthermore, the states have been augmented for each electron by plane-wave electron translation factors to ensure Galilean invariance of the results (see [42]). The two collision systems can then be described using an *ab initio* representation, which allows for the accurate description of C^{4+} (O^{6+}) and, after electron transfer, C^{3+} (O^{5+}) states, including spatial and spin components (but neglecting spin-orbit coupling). However, for the target, one of the He electrons is frozen so that the interactions between the He^+ core and the three active electrons is described by a model potential (see Table III in [42]). For the static (state and basis sets construction) and dynamical (collision) stages of the calculations, all Coulombic interactions and bi-electronic couplings were taken into account within a full configuration interaction scheme.

The method has been described in detail previously [46–48] and already used for single-electron capture [36,42] and transfer-excitation [43] investigations in C^{4+}-He (and H_2) MeV collisions. In these previous works, we chose a nonperturbative approach using very large basis sets to simultaneously describe one-electron processes (transfer, excitation, and, in a more limited way, ionization) and two-electron processes (mainly transfer excitation and double excitation). The present results, therefore, stem from the same computations for C^{4+} projectiles using the same sets of Gaussian-type orbitals (GTOs) for the genuine representation of the helium and carbon states. For oxygen projectiles, we have an equivalent representation of the O^{6+} and O^{5+} states, with a set of 22 GTOs, i.e., 10 for $\ell = 0$ and 3×4 $\ell = 1$ symmetries. The energies of the projectile states under consideration in the present work for the C^{4+} and O^{6+} ions were compared to reference values, with an agreement better than ~0.9% for carbon and ~0.5% for oxygen. The target is described by the same GTO base as in [42], with the ground state bound by 0.901 a.u. (to be compared to the NIST value of 0.904 a.u. [49]).

For C^{4+}+He collisions, to solve the time-dependent Schrödinger equation, the expansion of the scattering state spans the same Hilbert space as in [42], i.e., with a total of 1794 three-electron bound, autoionizing, and continuum states (799 of type $C^{4+} \times$ He and 995 of type C^{3+}) for doublet spin symmetry ($802 = 380 + 422$ for quartet, respectively). For O^{6+}+He collisions, the basis set includes 1357 three-electron states, with 694 of $O^{6+} \times$ He and O^{5+} types,

for doublet spin symmetry ($598 = 322 + 276$ for quartet, respectively).

The cross sections stemming from these close-coupling computations, shown in the following, are inclusive cross sections, i.e., cross sections for excitation to ($2s2p\ ^3P$) from all possible final states of the helium target [see Eq. (1)]. This is mandatory since (i) the target is not analyzed experimentally after collision and (ii) our calculations indicate that He excitation and ionization are important channels for initially metastable ($1s2s\ ^{1,3}S$) He-like ions. The cross sections for the production of excited and ionized He, with the projectile staying in its initial state, are indeed about two orders of magnitude larger for C^{4+} collisions (and even more so for O^{6+}) than those for the processes under consideration, so that we have been careful to include the simultaneous inelastic processes acting on both centers in the cross sections presented in the following.

B. Plane-wave Born approximation (PWBA)

To date, most of our understanding of excitation in atomic collisions, particularly in first-row few-electron ions and atoms, has come predominantly from PWBA calculations performed in the independent electron approximation using hydrogenic wave functions [32,50]. The first-order Born ($B1$) excitation cross section $\sigma^{B1}(P: i \to f, T: 0 \to n)$, where a projectile of atomic number Z_p (or $Z_p^\star$ if screening is used) with N_p electrons is excited from state i to f and a target of atomic number Z_t (or $Z_t^\star$ if screening is used) with N_t electrons, is simultaneously excited from state 0 to n (also spanning the continuum) is given in atomic units (a.u.) by

$$\sigma^{B1}(P: i \to f, T: 0 \to n) = \frac{1}{2\pi V_p^2} \int_{q_{\min}}^{q_{\max}} q\, dq\, |\langle fn| V |0i\rangle|^2, \tag{4}$$

where V_p is the projectile velocity and q the momentum transfer. $\langle fn| V |0i\rangle$ is the PWBA excitation amplitude, with V the perturbation [51] given, for example, for $N_p = 1$ and $N_t = 2$ by

$$V = \frac{Z_p^\star Z_t^\star}{R} - \frac{Z_t^\star}{|\mathbf{R} + \mathbf{r}_{p1}|} - \frac{Z_p^\star}{|\mathbf{R} - \mathbf{r}_{t1}|} - \frac{Z_p^\star}{|\mathbf{R} - \mathbf{r}_{t2}|} + \frac{1}{|\mathbf{R} - \mathbf{r}_{t1} + \mathbf{r}_{p1}|} + \frac{1}{|\mathbf{R} - \mathbf{r}_{t2} + \mathbf{r}_{p1}|}, \tag{5}$$

where $\mathbf{R}$ is the internuclear vector and $\mathbf{r}_{p1}$, $\mathbf{r}_{t1}$, and $\mathbf{r}_{t2}$ are the electron position vectors with respect to their corresponding nuclear centers. Application to projectile $1s \to 2p$ excitation results in the following well-known [32,51,52] cross sections (in a.u.):

$$\sigma^{B1}(P: 1s \to 2p,\ T: 1s \to 1s) = \frac{8\pi}{V_p^2} \int_{q_0}^{\infty} \frac{dq}{q^3} \left|N_p\, \mathcal{G}^P(q/Z_p^\star, 1s \to 2p)\right|^2 \left|Z_t^\star - N_t\, \mathcal{G}^T(q/Z_t^\star, 1s \to 1s)\right|^2, \tag{6}$$

$$\sigma^{B1}\left(P: 1s \to 2p,\ T: 1s \to \sum_{\text{exc}}\right) = \frac{8\pi}{V_p^2} \int_{q_0+\delta}^{\infty} \frac{dq}{q^3} \left|N_p\, \mathcal{G}^P(q/Z_p^\star, 1s \to 2p)\right|^2 \left\{N_t\, [1 - \left|\mathcal{G}^T(q/Z_t^\star, 1s \to 1s)\right|^2]\right\}, \tag{7}$$

where $\sum_{\text{exc}}$ in Eq. (7) represents the sum over all *excited and continuum* states of the target. This sum has been evaluated on the right-hand side of the equation using the closure approximation. In the lower limits of the two integrals, $q_0 = \Delta\epsilon^P/V_p$ is the minimum momentum transfer, where $\Delta\epsilon^P$ is the projectile $1s \to 2p$ excitation energy, while δ is a parameter introduced in the closure approximation [53].

The form factors $\mathcal{G}^{P(T)}$ are matrix elements of the projectile and target [51], respectively, defined, in general, as

$$\mathcal{G}^{P(T)}(q/Z^\star, i \to f) \equiv \int \psi_f^{\star P(T)}(Z^\star, \mathbf{r}) e^{i\mathbf{r}\cdot\mathbf{q}} \psi_i^{P(T)}(Z^\star, \mathbf{r}) d\mathbf{r}, \tag{8}$$

where $\psi_f^{P(T)}(Z^\star, \mathbf{r})$ and $\psi_i^{P(T)}(Z^\star, \mathbf{r})$ are either projectile (P) or target (T) hydrogenic wave functions of the initial state i (0) or final state f (n), respectively, with the screened nuclear charge $Z^\star$ (either $Z_p^\star$ and $Z_t^\star$ accordingly). These form factors are readily evaluated analytically for the projectile $1s \to 2p$ and target $1s \to 1s$ cases [32,51,54]. When more than one electron is used, the appropriate screening can be applied.

An interesting and unique feature of the PWBA is the separation of the excitation amplitude $\langle fn| V |0i\rangle$ into a product of one term which depends only on the projectile wave functions and a second term which depends only on the target. This separation is important as it allows considerable simplification in the evaluation of the target contributions through the closure approximation. The two mechanisms represented by Eqs. (6) and (7) are shown schematically in Figs. 2(a) and 2(b), respectively. The sum of both cross sections represents the total contribution of the target, He(All). The primary contribution to the $1s \to 2p$ projectile excitation cross section [Eq. (6)] is seen in Fig. 2(a) to be due to the N_p projectile electrons interacting with the target nuclear charge Z_t [an $(e - n)$ interaction] whose strength, however, is reduced by the screening action of the surrounding N_t target electrons. In the PWBA, this is known as the *screening* contribution. The target remains in its initial state [51] and thus this process involves just a *single* excitation in the collision.

The second contribution [Eq. (7)] is seen to be due to the $(e - e)$ interaction between the N_p projectile electrons and the N_t target electrons [also known as two-center $(e - e)$ interactions or TC*ee* [55]; see Fig. 2(b)]. The interacting target electron is also excited or ionized [32], resulting in a *double* excitation (of both the projectile and target) in the collision [32]. In the PWBA, this is known as the *antiscreening* [51]

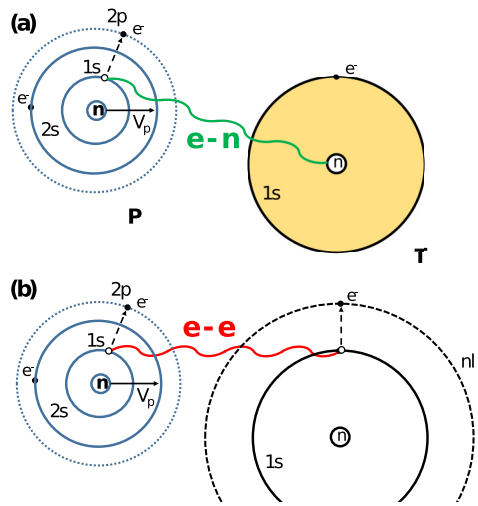

FIG. 2. Schematic of the $1s \to 2p$ projectile excitation first-order mechanisms in collisions of a He-like $1s2s$ open-shell ion (P) with a He target (T) resulting in the $2s2p$ projectile configuration. Only one electron is shown on the target for simplicity. The projectile excitation is mediated by the interaction of the projectile electron with the target: (a) nuclear charge in a $(e-n)$ interaction (green wiggly line), which is, however, screened (as denoted by the yellow-shaded area) by the target electron which remains in its ground state; (b) electron in a $(e-e)$ interaction (red wiggly line), where the target electron is also excited to the nl orbital (where n can also be in the continuum). First-order processes (a) and (b) are treated by the PWBA [Eqs. (6) and (7)] and referred to as the screening and antiscreening mechanisms, respectively.

contribution. It is then clear that in this first-order theory, the simultaneous excitation of both projectile and target is *only* possible via such TC*ee* interactions [13,51]. The E_p energy dependence of the antiscreening cross section is also quite different from that of the screening one. Antiscreening exhibits a distinct threshold behavior rising sharply at much larger E_p energies [25,56–58] than screening. This threshold behavior has been shown to be tied to the projectile excitation energy $\Delta\epsilon^P$ [53] and has been linked to electron impact excitation in the quasifree electron scattering of the target electrons off the projectile causing its excitation [11,14,25,59].

We apply the above cross-section formulas with $N_p = 1$ to account for the one $1s$ electron in the $(1s2s\ ^3S)$ initial projectile state and $N_t = 2$ to account for the two equivalent $1s^2$ target electrons, using a screened nuclear charge of $Z_t^\star = 1.345$ [13]. We also use, for the $1s \to 2p$ projectile excitation energy $\Delta\epsilon^P$, the *actual* projectile $(1s2s\ ^3S) \to (2s2p\ ^3P)$ excitation energies, i.e., 13.2 a.u. for carbon and 23.6 a.u. for oxygen, instead of the hydrogenic ones, in an effort to further improve the calculations. Thus, a screened projectile nuclear charge, in analogy to the energy of a hydrogenic $1s-2p$ transition, is computed as $Z_p^\star = \sqrt{8\Delta\epsilon^P/3}$ [7.933 for $O^{6+}(1s2s)$ and 5.932 for $C^{4+}(1s2s)$, respectively] to account for the screening by the additional $2s$ electron.

It is clear that the above first-order Born formulas do not account for the spin of the states, nor do they include exchange or antisymmetry. They also do not include any configuration interactions or strictly address the excitation of autoionizing states. Nevertheless, the PWBA approach, with all of its shortcomings, has, to date, provided our main insight to excitation and loss through the two mechanisms of screening and antiscreening. If the first-order treatment is valid, these mechanisms could, in principle, be distinguished if the final state of the target can be determined. In the former, the target is unexcited, while in the latter, it is excited or even ionized. To date, *only loss* experiments, in which the ionized projectile is recorded in coincidence with the recoiling ionized He target, have been able to distinguish between contributions from the He ground state and the He^+ final states of the target [57,58,60,61]. In the present work focusing on projectile excitation, the final states of the He target are *not* distinguished experimentally. However, they are distinguished in our 3eAOCC calculations. Comparison to the PWBA results is thus of interest and discussed.

C. Auger angular distributions

The theoretical projectile frame $2s2p\ ^3P$ Auger SDCSs at $\theta = 0^\circ$ are given by [27,62]

$$\frac{d\sigma_A}{d\Omega'}(0^\circ) = \bar{\xi}\,\frac{(1+2D_2)\sigma[M=0] + 2(1-D_2)\sigma[M=1]}{4\pi}. \tag{9}$$

Here, $\sigma[M]$ are the M-dependent partial excitation cross sections, which are functions of the projectile energy E_p and the azimuthal quantum number M. In the considered LS coupling for the $2s2p\ ^3P$ state, we have $L = 1$ and $M = 0, 1$. $\bar{\xi}$ is the LSJ-averaged Auger yield. D_2 is the dealignment factor, which accounts for the average loss of orbital alignment into spin alignment in the partially overlapping LSJ multiplets $(2s2p\ ^3P_{2,1,0})$ and was calculated according to the formulation given in Mehlhorn and Taulbjerg [62]. For the $2s2p\ ^3P_{2,1,0}$ Auger decay, we obtain, using published fine-structure results, $\bar{\xi} = 0.951$ and $D_2 = 0.321$ for carbon [63] and $\bar{\xi} = 0.850$ and $D_2 = 0.283$ for oxygen [64].

Finally, assuming isotropic Auger emission, we have

$$\frac{d\sigma_A}{d\Omega'}(0^\circ) = \bar{\xi}\,\frac{\sigma_{\rm tot}}{4\pi}\ \ \text{(isotropy)}, \tag{10}$$

where $\sigma_{\rm tot} = \sigma[M=0] + 2\sigma[M=1]$ is the total excitation cross section. This is seen to be equivalent to setting $D_2 = 0$ in Eq. (9).

IV. RESULTS AND DISCUSSION

A. Comparison of single-differential cross sections

In Fig. 3, we present the main results of this work, the measured $\theta = 0^\circ$ Auger SDCS for $2s2p\ ^3P$ projectile excitation of C^{4+} and O^{6+} projectiles in collisions with helium and the corresponding 3eAOCC calculations. The 3eAOCC results represent the state of the art in our theoretical ability to address excitation in a nonperturbative, close-coupling multielectronic approach. The cross sections for the two collision systems present significant differences with a maximum at about 0.6 MeV/u for the carbon projectile, while the maximum is not yet reached at 1.5 MeV/u for oxygen due to the larger (about a factor of 1.8) Q value of the considered oxygen

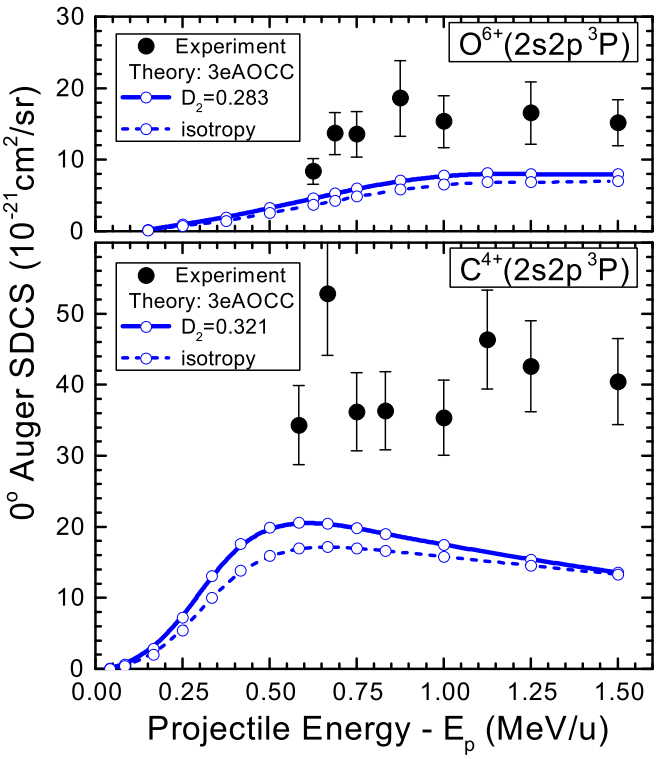

FIG. 3. Absolute, 0° Auger single-differential cross sections $[d\sigma_A(0^\circ)/d\Omega']$, for production of the $(2s2p\ ^3P)$ from the $(1s2s\ ^3S)$ initial state of C^{4+} (bottom) and O^{6+} (top) projectiles in collisions with He. Experiment: Black filled circles with error bars. Theory: Blue open circles connected by lines. The 3eAOCC results including all possible final He states considered in the basis are shown as solid lines for dealignment factor D_2 [Eq. (9)] and as dashed lines for the isotropic hypothesis [Eq. (10)].

excitation channel. In Table I, we also tabulate the results used to generate Fig. 3.

As can be seen in Fig. 3, the calculated 3eAOCC SDCSs for both ions are smaller, within a factor of 1.5–2 of the measured SDCSs and in reasonable agreement as to their projectile energy dependence. Note that calculations using the dealignment parameter D_2 [Eq. (9)] or assuming isotropy [Eq. (10)] are indicated, with the differences seen to be rather small, justifying the assumption of isotropy used in the past.

In the measured SDCSs shown in Fig. 3, the observed error bars include the uncertainty in the determined metastable fraction $f[^3S]$ added in quadrature to the statistical uncertainty of the Auger data. For oxygen, the uncertainty in $f[^3S]$ varied around 19–28%, while for carbon, it varies around 15%. The statistical errors determined from the fitted DDCSs for oxygen were much smaller, mostly varying from 10% at the lower energies to about 2% at the highest, while similarly for carbon, from 6% to about 0.7%. Going lower in energy than about 0.5 MeV/u becomes increasingly difficult due to the low ion-beam intensities (a few tens of pA on target). For these highly charged ions at the lowest collision energies, poststripping is required, which further degrades beam quality introducing energy straggling, which also affects the energy resolution of the Auger spectra [65].

In the theoretical SDCSs shown in Fig. 3, the absolute uncertainty is expected to be 20% at maximum, as also reported for capture and transfer excitation in Refs. [36,42,43], using different sets of GTOs to express (i) the target and projectile states and (ii) the atomic states included in the coupled-channel calculations. The differences between the experimental and theoretical cross sections cannot be simply explained by the uncertainties related to these series of data and are difficult to interpret. Even if we cannot, in principle, rule out systematic errors (although the greatest care has been taken in the acquisition and analysis of both experimental and theoretical results), it is in the modeling of these collision systems that we may try to find a possible explanation for this disagreement. But first we exclude cascade effects, which could make the comparison between theory and experiment less straightforward.

B. Cascades

Since our experimental cross sections are seen to be consistently larger than theory, the question as to whether this could be due to *cascades* arises. Radiative cascade feeding is a well-known problem in Li-like levels (see [66] and references therein) that also affects levels of H-like ions [30,67]. For example, $2p$ projectile states can be fed by dipole (E1) transitions from higher-lying nl-excited projectile states, which can have a large fluorescence yield for feeding the $2p$ level (as, for example, from the $3s$ or $3d$ levels). In the case of low-Z_p He-like projectile levels though, the production of the $2s2p\ ^3P$, which can be fed from higher-lying $2snl\ ^3L$ levels by E1 cascades, has a rather low fluorescence yield [68] since they can also Auger decay strongly to the $1s$ ground state, an option not available to H-like projectile levels. Goryaev *et al.* [64] give maximum fluorescence yields of $\lesssim 5\%$ for carbon and $\lesssim 8\%$ for oxygen $2s3l$ doubly excited states, which are indeed quite small and thus cannot account for the difference in the SDCSs between theory and experiment.

C. 3eAOCC comparison between He and He^+ targets

The semiclassical approach, the quality of the important states, the convergence level of the calculations, and the numerics in themselves cannot be suspected to be the reason behind the lower values of the 3eAOCC results compared to the measured cross sections. One should then turn to the number of electrons kept active in the model. For the two projectiles, our approach includes all active electrons, with two active electrons initially, and even three during the collision to also account for any transfer processes. This, however, is not the case for the helium target, for which only one electron is active, the other being included passively to screen the nuclear charge through a model potential [36]. What should be the effect of this second electron on our process? One can only speculate on this since, at present, four-electron calculations are out of reach (due to CPU and memory requirements) when considering an initially excited state such as the $1s2s\ ^3S$. Using simple qualitative arguments, one could state that this second electron (i) would have hardly any effect if the excitation was mainly driven by the electron-nucleus interaction, and (ii) would multiply the cross sections by two if, alternatively, the two-center electron-electron interactions induce

TABLE I. Main results for the production of the $2s2p\ ^3P$ state in collisions of He-like carbon and oxygen with helium. The experimental SDCS, $d\sigma_A^{\rm exp}(0^\circ)/d\Omega'$, and the theoretical SDCS, $d\sigma_A(0^\circ)/d\Omega'$, are compared in Fig. 3, while the 3eAOCC total cross sections, $\sigma_{\rm tot}$, are shown as the thick blue line in Fig. 4. Either one or two strippers were used, designated as FTS: foil terminal stripping; GTS: gas terminal stripping; FPS: foil poststripping; and GPS: gas poststripping.

					Theory: 3eAOCC					Experiment	
								$d\sigma_A(0^\circ)/d\Omega'$			
V_p	E_p		Stripping	$f[^3S]$[a]	$\sigma[M=0]$	$\sigma[M=1]$	$\sigma_{\rm tot}$[b]	D_2[c]	Isotropy[d]	$dY_A^{\rm exp}(0^\circ)/d\Omega'$	$d\sigma_A^{\rm exp}(0^\circ)/d\Omega'$[e]
(a.u.)	(MeV)	(MeV/u)		(%)	($\times 10^{-21}$ cm^2)			($\times 10^{-21}$ cm^2/sr)		($\times 10^{-21}$ cm^2/sr)	
					$C^{4+}(1s2s\ ^3S) + He \rightarrow C^{4+}(2s2p\ ^3P)$+He(All)						
1.291	0.500	0.0417			0.336	0.0617	0.459	0.0481	0.0348		
1.826	1.00	0.0833			4.95	0.437	5.82	0.660	0.441		
2.582	2.00	0.167			20.6	3.03	26.7	2.87	2.02		
3.162	3.00	0.250			48.7	10.7	70.2	7.16	5.31		
3.652	4.00	0.333			86.1	23.2	132	13.1	10.0		
4.082	5.00	0.417			113	35.0	183	17.6	13.8		
4.472	6.00	0.500	GTS-GPS	13.4 ± 2.0	124	43.7	211	19.9	16.0		
4.830	7.00	0.583	GTS-GPS	(14.2 ± 2.1)	125	49.3	224	20.6	16.9	4.89 ± 0.30	34.3 ± 5.6
5.164	8.00	0.667	GTS-GPS	(14.2 ± 2.1)	121	52.9	227	20.5	17.2	7.49 ± 0.52	52.8 ± 8.7
5.477	9.00	0.750	GTS-GPS	14.1 ± 2.1	114	55.2	224	19.8	17.0	5.11 ± 0.12	36.2 ± 5.5
5.774	10.0	0.833	GTS-GPS	(16.7 ± 2.5)	106	56.8	220	19.1	16.6	6.05 ± 0.13	36.3 ± 5.5
6.325	12.0	1.000	FTS	17.6 ± 2.6	92.0	58.5	209	17.4	15.8	6.21 ± 0.052	35.4 ± 5.3
6.709	13.5	1.125	FTS	(17.5 ± 2.6)						8.10 ± 0.057	46.3 ± 7.0
7.071	15.0	1.250	FTS	11.5 ± 1.7	75.3	58.6	192	15.4	14.6	4.91 ± 0.035	42.6 ± 6.4
7.746	18.0	1.500	FTS	(11.4 ± 1.7)	62.6	56.6	176	13.6	13.3	4.62 ± 0.027	40.4 ± 6.1
					$O^{6+}(1s2s\ ^3S) + He \rightarrow O^{6+}(2s2p\ ^3P)$+He(All)						
2.449	2.40	0.150			1.42	0.258	1.94	0.176	0.131		
3.162	4.00	0.250			8.22	1.34	10.9	1.00	0.738		
3.873	6.00	0.375			15.5	3.11	21.7	1.95	1.47		
4.472	8.00	0.500	GTS-FPS	18.0 ± 4.0	25.1	6.12	37.4	3.25	2.53		
5.000	10.0	0.625	GTS-FPS	19.6 ± 3.8	33.9	9.86	53.7	4.55	3.63	1.64 ± 0.16	8.36 ± 1.8
5.244	11.0	0.687	GTS-FPS	20.2 ± 3.9	38.7	12.0	62.6	5.26	4.23	2.76 ± 0.26	13.7 ± 2.9
5.477	12.0	0.750	GTS-FPS	20.0 ± 4.5	43.2	14.1	71.3	5.94	4.83	2.70 ± 0.16	13.5 ± 3.2
5.916	14.0	0.875	FTS-FPS	16.0 ± 4.5	50.1	18.0	86.0	7.05	5.82	2.97 ± 0.12	18.6 ± 5.3
6.325	16.0	1.000	GTS-FPS	17.6 ± 4.0	53.8	21.0	95.8	7.73	6.48	2.70 ± 0.19	15.3 ± 3.7
6.709	18.0	1.125			55.0	23.2	101	8.07	6.85		
7.071	20.0	1.250	FTS	14.5 ± 3.8	52.9	24.1	101	7.95	6.84	2.40 ± 0.072	16.5 ± 4.4
7.746	24.0	1.500	FTS	17.5 ± 3.7	51.1	26.3	104	7.96	7.01	2.65 ± 0.053	15.1 ± 3.2

[a]Experimentally determined $f[^3S]$ using a three-component ion beam model including the ground- and the $1s2s\ ^1S$ metastable states. Values in parentheses are estimations based on interpolation.
[b]$\sigma_{\rm tot} = \sigma[M=0] + 2\sigma[M=1]$.
[c]Eq. 9 with $D_2 = 0.321$, $\overline{\xi} = 0.951$ for carbon and $D_2 = 0.281$, $\overline{\xi} = 0.850$ for oxygen.
[d]Eq. 10 with previous Auger yields $\overline{\xi}$.
[e]Eq. 3 with the overall uncertainty computed from the statistical uncertainty of $dY_A^{\rm exp}(0^\circ)/d\Omega'$ and the $f[^3S]$ uncertainty added in quadrature.

the excitation process. However, these two cases cannot be taken as strict lower and upper limits of the possible effect on our 3eAOCC results since this perturbativelike argument cannot hold in a close-coupling scheme, where channels can be tightly coupled and their contributions are included coherently.

In order to further investigate the effects of the $(e-e)$ and $(e-n)$ interactions responsible for excitation, we have performed additional coupled-channel calculations for the same projectiles, but with a He^+ target. Here, we have again only one electron on the target, but no screening is required as in the case of the *neutral* He model target.

In Table II, we report on the total $2s2p\ ^3P$ excitation cross sections, $\sigma_{\rm tot}$, for the two targets He and He^+, at four typical impact energies. The two 3eAOCC cross sections appear surprisingly close, with differences of less than 25%. This fact tends to show that the target nuclear charge is *not* the determinative parameter in the excitation process and that the two-center bi-electronic couplings are important. We may therefore speculate that coupled-channel calculations including an additional (second) target electron (i.e., in a *four*-electron approach) would give higher cross sections, possibly bridging the gap between the present experimental and theoretical SDCSs.

TABLE II. Total cross sections σ_{tot} for $(2s2p\ ^3P)$ excitation in collisions of $(1s2s\ ^3S)$ O^{6+} and C^{4+} ions with He and He^+ one-electron targets. Indicated cross sections are from 3eAOCC calculations and correspond to the sum of both ground and excited states of the target (including ionization), He(All) and He^+(All).

		σ_{tot} $(10^{-20}cm^2)$			
V_p	E_p	O^{6+}		C^{4+}	
(a.u.)	(MeV/u)	He[a]	He^+	He[a]	He^+
5.000	0.625	5.37	4.21	22.6	21.7
5.477	0.750	7.13	5.94	22.4	23.5
6.325	1.000	9.58	8.86	20.9	24.8
7.071	1.250	10.1	10.3	19.2	24.6

[a]Shown as He(All) in Fig. 4 (blue continuous lines).

D. Contributions from the ground and excited states of the target

In Fig. 4, we compare, for the $2s2p\ ^3P$ excitation channel, the separate contributions from the target ground state [He(gs)] and excited state [He(exc + ion)] as a function of impact energy for both oxygen (top) and carbon (bottom) projectiles in collisions with He. These are compared to the PWBA He (with $N_t = 2$) results corresponding to the screening and antiscreening terms in Eqs. (6) and (7), respectively. Also shown is the sum of the two contributions [He(All)].

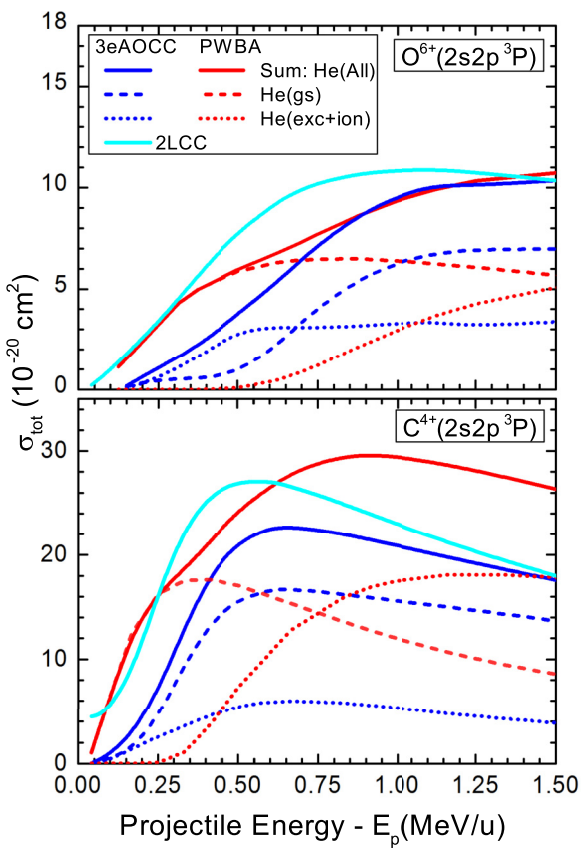

FIG. 4. Total cross sections σ_{tot} showing the separate contributions from the ground- and excited- state (including ionization) target contributions. Blue lines: 3eAOCC calculations. Red lines: PWBA calculations. Dashed lines: He(gs) ground-state contributions. Dotted lines: He(exc + ion) excited- and ionized-state contributions. Continuous lines: He(All) = Sum of both He(gs) and He(exc + ion) contributions. Two-level 3eAOCC (2LCC) results are also shown as the azure lines.

The PWBA results, including all target contributions He(All), are seen to be mostly larger than the 3eAOCC results, with the main target contributions in both calculations deriving predominantly from the target ground state, He(gs). The E_p dependence of σ_{tot} is seen to be very similar for both results above about 0.75 MeV/u. However, this dependence is seen to be quite different at the lower collision energies, with the PWBA He(gs) contributions dropping faster with decreasing E_p than those of the 3eAOCC, and also peaking at lower E_p. On the other hand, the PWBA He(All), peaks later than the 3eAOCC.

For the excited-ionized target contributions He(exc + ion), the PWBA results show the characteristic $(e - e)$ threshold behavior [57] associated with the antiscreening process, rising rapidly (above 0.25 MeV/u for carbon and above 0.5 MeV/u for oxygen) and then saturating. These different $(e - e)$ threshold energies are related to the different $2s2p\ ^3P$ projectile excitation energies $\Delta\epsilon^P$ of the two ions, already mentioned. Interestingly, these thresholds are *not* observed in our results shown in Figs. 3 and 4, for either experimental or theoretical (3eAOCC). In qualitative agreement, the older ZAPS measurements of $2s2p\ ^3P$ projectile excitation for the similar F^{7+}+ He/H_2 collision systems also did *not* show any such $(e - e)$ thresholds [26]. This unobserved threshold behavior is clearly puzzling as it has been an important feature of our general understanding to date of either loss or excitation, based on the PWBA and TC*ee* interactions (see [11,14,15,69,70] and references therein).

E. Two-level 3eAOCC calculations

To further investigate these results, we have also performed two-level 3eAOCC calculations (2LCC) in which only the initial $1s2s\ ^3S$ and final $2s2p\ ^3P$ projectile states, together with just the ground state of the target He, were included, i.e., excluding all other processes, such as electron capture. These are also shown in Fig. 4. The 2LCC results are seen to be larger than the ones from the full close-coupling calculations, and therefore somewhat closer to the results of the PWBA which is similarly derived from a two-state approximation. The large difference from the full calculations clearly show the effect of the close coupling with the other states, particularly at the lowest collision energies. It is only at the highest energies that both CC calculations are seen to converge, as expected.

These results indicate that the use of low-order perturbative treatments and related interpretations may be questionable in our energy range. In particular, the $(e - e)$ threshold behavior predicted by the first-Born approximation has only been clearly observed in *loss* coincidence experiments [57,58,60,61], where the TC*ee* could be isolated. In singles (as opposed to coincidence) measurements, only the excitation of the $1s2s2p\ ^4P$ in collisions of Li-like O^{5+} and F^{6+} ions with He/H_2 targets has shown such a clear threshold [25]. There, the ^4P state can only be formed via spin exchange, which

is only possible by electron exchange in TC*ee* interactions, while all $(e-n)$ interactions are blocked.

In the present work, spin exchange is not required for the production of the $2s2p\ ^3P$. However, other $(e-n)$ interactions, such as double $(e-n, e-n)$ interactions [71] not included in first-order perturbative treatments, but included in our 3eAOCC calculations, could give rise to the $2s2p\ ^3P$, while also exciting or ionizing the target. Such higher-order processes could mask the presence of the much weaker $(e-e)$ interactions and associated thresholds.

V. SUMMARY AND CONCLUSIONS

We have presented a nonperturbative, three-electron treatment of excitation in the production of $2s2p\ ^3P$ states in 0.5–1.5 MeV/u collisions of two-electron $C^{4+}(1s2s\ ^3S)$ and $O^{6+}(1s2s\ ^3S)$ ions with helium. The helium target was modeled by a single electron, while all couplings were included in a complete and coherent treatment. In parallel, the production of the $2s2p\ ^3P$ states was measured using 0° Auger projectile spectroscopy, with the $1s2s\ ^3S$ metastable component of the mixed-state beams also determined within the same measurement. This enabled absolute SDCSs comparisons between theory and experiment with the theoretical SDCSs found to be about a factor of 1.5–2 smaller than experiment, but with very similar projectile energy dependencies for both ions. A comparison between the coupled-channel results and those stemming from the long-established first-Born approximation is also provided. The limit of this latter approach is also discussed, through the comparison of basis restricted close-coupling calculations. This comparison for excitation provides an important advance in the modeling and understanding of multielectron multi-open-shell quantum systems under ultrafast perturbations. Further isoelectronic investigations, particularly of less asymmetric collision systems, are clearly of interest and will shed more light on these results and especially on the role of two-center $(e-e)$ interactions.

ACKNOWLEDGMENTS

We would like to thank the personnel of the "Demokritos" Tandem for their help with the measurements. We acknowledge support of this work by the project "CALIBRA/EYIE" (MIS 5002799) which is implemented under the Action "Reinforcement of the Research and Innovation Infrastructure," funded by the Operational Programme "Competitiveness, Entrepreneurship and Innovation" (NSRF 2014–2020) and co-financed by Greece and the European Union (European Regional Development Fund).

[1] A. K. Pradhan and S. N. Nahar, *Atomic Astrophysics and Spectroscopy* (Cambridge University Press, Cambridge, 2011).

[2] R. K. Janev, *Atomic and Molecular Processes in Fusion Edge Plasmas* (Springer, New York, 1995).

[3] M. R. C. McDowell, *Atomic and Molecular Processes in Controlled Thermonuclear Fusion*, NATO Science Series B (Springer, New York, 2012).

[4] S. J. A. Atawneh and K. Tőkési, Excitation cross sections in a collision between two ground-state hydrogen atoms, J. Phys. B **54**, 065202 (2021).

[5] A. Igarashi and D. Kato, Projectile angular distributions in $He^+ + H$ collisions, Phys. Scr. **99**, 015404 (2024).

[6] I. Bray, H. Hayat, D. V. Fursa, A. S. Kadyrov, A. W. Bray, and M. Cytowski, Calculations of electron scattering on H-like ions, Phys. Rev. A **101**, 022703 (2020).

[7] A. Müller, Electronion collisions: Fundamental processes in the focus of applied research, Adv. At. Mol. Opt. Phys. **55**, 293 (2008).

[8] A. C. K. Leung and T. Kirchner, Proton impact on ground and excited states of atomic hydrogen, Eur. Phys. J. D **73**, 246 (2019).

[9] K. H. Spicer, C. T. Plowman, I. B. Abdurakhmanov, A. S. Kadyrov, I. Bray, and S. U. Alladustov, Differential study of proton-helium collisions at intermediate energies: Elastic scattering, excitation, and electron capture, Phys. Rev. A **104**, 032818 (2021).

[10] J. Faulkner, I. B. Abdurakhmanov, S. U. Alladustov, A. S. Kadyrov, and I. Bray, Electron capture, excitation and ionization in $He^{2+} - H$ and $H^+ - He^+$ collisions, Plasma Phys. Control. Fusion **61**, 095005 (2019).

[11] T. J. M. Zouros, Projectile-electron - target-electron interactions: Exposing the dynamic role of electrons in fast ion-atom collisions, Comments At. Mol. Phys. **32**, 291 (1996).

[12] D. H. Madison and E. Merzbacher, Theory of charged particle excitation, in *Atomic Inner-Shell Processes, Vol I: Ionization and Transition Probabilities*, edited by B. Crasemann (Academic Press, New York, 1975), pp. 1–72.

[13] J. S. Briggs and K. Taulbjerg, Theory of inelastic atom-atom collisions, in *Topics in Current Physics, Vol. 5: Structure and Collisions of Ions and Atoms*, edited by I. A. Sellin (Springer Verlag, Berlin, 1978), pp. 105–153.

[14] E. C. Montenegro, W. E. Meyerhof, and J. H. McGuire, Role of two-center electron-electron interaction in projectile electron excitation and loss, Adv. At. Mol. Opt. Phys. **34**, 249 (1994).

[15] T. J. M. Zouros, Excitation and ionization in fast ion-atom collisions due to projectile electron–target electron interactions, in *Applications of Particle and Laser Beams in Materials Technology*, Vol. 283, edited by P. Misailides, *NATO Advanced Study Institute Series E: Applied Sciences* (Kluwer Academic, Netherlands, 1995), pp. 37–52.

[16] N. Stolterfoht, R. D. Dubois, and R. D. Rivarola, *Electron Emission in Heavy Ion-Atom Collisions*, Springer Series on Atomic, Optical and Plasma Physics (Springer, Berlin, 1997).

[17] B. Najjari and A. B. Voitkiv, Excitation of heavy hydrogenlike ions by light atoms in relativistic collisions with large momentum transfers, Phys. Rev. A **85**, 052712 (2012).

[18] F. Hopkins, R. L. Kauffman, C. W. Woods, and P. Richard, *K* x-ray transitions in one- and two-electron oxygen and fluorine projectiles produced in helium, neon, and argon targets, Phys. Rev. A **9**, 2413 (1974).

[19] F. Hopkins, A. Little, and N. Cue, Inner-shell Coulomb excitation in the collisions of few-electron F with H_2 and He, Phys. Rev. A **14**, 1634 (1976).

[20] D. Detleffsen, M. Anton, A. Werner, and K.-H. Schartner, Excitation of atomic hydrogen by protons and multiply charged ions at intermediate velocities, J. Phys. B **27**, 4195 (1994).

[21] D. Vernhet, L. Adoui, J. P. Rozet, K. Wohrer, A. Chetioui, A. Cassimi, J. P. Grandin, J. M. Ramillon, M. Cornille, and C. Stephan, Multielectron processes in heavy ion-atom collisions at intermediate velocity, Phys. Rev. Lett. **79**, 3625 (1997).

[22] E. Träbert and I. Martinson, 2.4 MeV C^{q+} on He: Inverse reaction for active diagnostics of future fusion plasmas, Phys. Scr. **57**, 109 (1998).

[23] M. Terasawa, T. J. Gray, S. Hagmann, J. Hall, J. Newcomb, P. Pepmiller, and P. Richard, Electron capture by and electron excitation of two-electron fluorine ions incident on helium, Phys. Rev. A **27**, 2868 (1983).

[24] T. R. Dillingham, J. Newcomb, J. Hall, P. L. Pepmiller, and P. Richard, Projectile *K*-Auger-electron production by bare, one-, and two-electron ions, Phys. Rev. A **29**, 3029 (1984).

[25] T. J. M. Zouros, D. H. Lee, and P. Richard, Projectile $1s \rightarrow 2p$ excitation due to electron-electron interaction in collisions of O^{5+} and F^{6+} ions with H_2 and He targets, Phys. Rev. Lett. **62**, 2261 (1989).

[26] D. H. Lee, P. Richard, J. M. Sanders, T. J. M. Zouros, J. L. Shinpaugh, and S. L. Varghese, Electron capture and excitation studied by state-resolved KLL Auger measurement in 0.25–2 MeV/u $F^{7+}(1s^2\,{}^1S,\ 1s2s\,{}^3S)$+$H_2$/He collisions, Nucl. Instrum. Methods Phys. Res., Sect. B **56–57**, 99 (1991).

[27] N. Stolterfoht, A. Mattis, D. Schneider, G. Schiwietz, B. Skogvall, B. Sulik, and S. Ricz, Time-ordering effects in *K*-shell excitations of 170-MeV Ne^{7+} colliding with gas atoms: Single excitation, Phys. Rev. A **48**, 2986 (1993).

[28] N. Stolterfoht, A. Mattis, D. Schneider, G. Schiwietz, B. Skogvall, B. Sulik, and S. Ricz, Time-ordering effects in *K*-shell excitation of 170-MeV Ne^{7+} colliding with gas atoms: Double excitation, Phys. Rev. A **51**, 350 (1995).

[29] A. Gumberidze, D. B. Thorn, C. J. Fontes, B. Najjari, H. L. Zhang, A. Surzhykov, A. Voitkiv, S. Fritzsche, D. Banaś, H. Beyer, W. Chen, R. D. DuBois, S. Geyer, R. E. Grisenti, S. Hagmann, M. Hegewald, S. Hess, C. Kozhuharov, R. Märtin, I. Orban, N. Petridis, R. Reuschl, A. Simon, U. Spillmann, M. Trassinelli, S. Trotsenko, G. Weber, D. F. A. Winters, N. Winters, D. Yu, and T. Stöhlker, Electron- and proton-impact excitation of hydrogenlike uranium in relativistic collisions, Phys. Rev. Lett. **110**, 213201 (2013).

[30] A. Gumberidze, D. B. Thorn, A. Surzhykov, C. J. Fontes, D. Banaś, H. F. Beyer, W. Chen, R. E. Grisenti, S. Hagmann, R. Hess, P.-M. Hillenbrand, P. Indelicato, C. Kozhuharov, M. Lestinsky, R. Märtin, N. Petridis, R. V. Popov, R. Schuch, U. Spillmann, S. Tashenov, S. Trotsenko, A. Warczak, G. Weber, W. Wen, D. F. A. Winters, N. Winters, Z. Yin, and T. Stöhlker, Angular distribution of characteristic radiation following the excitation of He-like uranium in relativistic collisions, Atoms **9**, 20 (2021).

[31] D. R. Bates and G. Griffing, Inelastic collisions between heavy particles I: Excitation and ionization of hydrogen atoms in fast encounters with protons and with other hydrogen atoms, Proc. Phys. Soc. Sect. A **66**, 961 (1953).

[32] D. R. Bates and G. Griffing, Inelastic collisions between heavy particles II: Contributions of double-transitions to the cross sections associated with the excitation of hydrogen atoms in fast encounters with other hydrogen atoms, Proc. Phys. Soc. Sect. A **67**, 663 (1954).

[33] W. Fritsch and C. D. Lin, The semiclassical close-coupling description of atomic collisions: Recent developments and results, Phys. Rep. **202**, 1 (1991).

[34] J. B. Wang, J. P. Hansen, and A. Dubois, Spin anisotropy for excitation in collisions between two one-electron atoms, Phys. Rev. Lett. **85**, 1638 (2000).

[35] A. Igarashi and D. Kato, Cross sections in $He^+ + H$ collisions for the energy region 1-100 keV u^{-1}, Phys. Scr. **98**, 055402 (2023).

[36] I. Madesis, A. Laoutaris, T. J. M. Zouros, E. P. Benis, J. W. Gao, and A. Dubois, Pauli shielding and breakdown of spin statistics in multielectron multi-open-shell dynamical atomic systems, Phys. Rev. Lett. **124**, 113401 (2020).

[37] S. Harissopulos, M. Andrianis, M. Axiotis, A. Lagoyannis, A. G. Karydas, Z. Kotsina, A. Laoutaris, G. Apostolopoulos, A. Theodorou, T. J. M. Zouros, I. Madesis, and E. P. Benis, The Tandem Accelerator Laboratory of NCSR "Demokritos": current status and perspectives, Eur. Phys. J. Plus **136**, 617 (2021).

[38] E. P. Benis, I. Madesis, A. Laoutaris, S. Nanos, and T. J. M. Zouros, Mixed-state ionic beams: An effective tool for collision dynamics investigations, Atoms **6**, 66 (2018).

[39] E. P. Benis and T. J. M. Zouros, Determination of the $1s2\ell2\ell'$ state production ratios ${}^4P^o/{}^2P$, ${}^2D/{}^2P$ and ${}^2P_+/{}^2P_-$ from fast $(1s^2,\ 1s2s\,{}^3S)$ mixed-state He-like ion beams in collisions with H_2 targets, J. Phys. B **49**, 235202 (2016).

[40] T. J. M. Zouros and D. H. Lee, Zero Degree Auger electron spectroscopy of projectile ions, in *Accelerator-Based Atomic Physics: Techniques and Applications*, edited by S. M. Shafroth and J. C. Austin (American Institute of Physics, Woodbury, NY, 1997), Chap. 13, pp. 426–479.

[41] I. Madesis, A. Laoutaris, T. J. M. Zouros, S. Nanos, and E. P. Benis, Projectile electron spectroscopy and new answers to old questions: Latest results at the new atomic physics beamline in Demokritos, Athens, in *State-of-the-Art Reviews on Energetic Ion-Atom and Ion-Molecule Collisions*, Interdisciplinary Research on Particle Collisions and Quantitative Spectroscopy, Vol. 2, edited by D. Belkić, I. Bray, and A. Kadyrov (World Scientific, Singapore, 2019), Chap. 1, pp. 1–31.

[42] I. Madesis, A. Laoutaris, S. Nanos, S. Passalidis, A. Dubois, T. J. M. Zouros, and E. P. Benis, State-resolved differential cross sections of single-electron capture in swift collisions of $C^{4+}(1s2s\,{}^3S)$ ions with gas targets, Phys. Rev. A **105**, 062810 (2022).

[43] A. Laoutaris, S. Nanos, I. Madesis, S. Passalidis, E. P. Benis, A. Dubois, and T. J. M. Zouros, Coherent treatment of transfer-excitation processes in swift ion-atom collisions, Phys. Rev. A **106**, 022810 (2022).

[44] C. W. Woods, R. L. Kauffman, K. A. Jamison, N. Stolterfoht, and P. Richard, *K*-shell Auger-electron production cross sections from ion bombardment, Phys. Rev. A **13**, 1358 (1976).

[45] S. Nanos, N. J. Esponda, P.-M. Hillenbrand, A. Biniskos, A. Laoutaris, M. A. Quinto, N. Petridis, E. Menz, T. J. M. Zouros, T. Stöhlker, R. D. Rivarola, J. M. Monti, and E. P. Benis, Cusp-electron production in collisions of open-shell He-like oxygen ions with atomic targets, Phys. Rev. A **107**, 062815 (2023).

[46] N. Sisourat, I. Pilskog, and A. Dubois, Nonperturbative treatment of multielectron processes in ion-molecule scattering: Application to He^{2+}-H_2 collisions, Phys. Rev. A **84**, 052722 (2011).

[47] J. W. Gao, Y. Wu, J. G. Wang, N. Sisourat, and A. Dubois, State-selective electron transfer in He^++He collisions at intermediate energies, Phys. Rev. A **97**, 052709 (2018).

[48] N. Sisourat and A. Dubois, Semiclassical close-coupling approaches, in *Ion-Atom Collision - The Few-Body Problem in Dynamic Systems*, edited by M. Schultz (de Gruyter, Berlin/Boston, 2019), pp. 157–178.

[49] A. Kramida, Y. Ralchenko, J. Reader, and NIST ASD Team, NIST Atomic Spectra Database (ver. 5.9), https://physics.nist.gov/asd (National Institute of Standards and Technology, Gaithersburg, MD, 2021).

[50] S. Ricz, B. Sulik, N. Stolterfoht, and I. Kádár, Semiclassical treatment of two-center electron-electron interactions in energetic atomic collisions: Screening effects, Phys. Rev. A **47**, 1930 (1993).

[51] J. H. McGuire, N. Stolterfoht, and P. R. Simony, Screening and antiscreening by projectile electrons in high-velocity atomic collisions, Phys. Rev. A **24**, 97 (1981).

[52] H. M. Hartley and H. R. J. Walters, Summing over excited states of the target in atomic collisions, J. Phys. B **20**, 1983 (1987).

[53] E. C. Montenegro and W. E. Meyerhof, Sum rules and electron-electron interaction in two-center scattering, Phys. Rev. A **43**, 2289 (1991).

[54] M. R. C. McDowell and J. P. Coleman, *Introduction to the Theory of Ion-Atom Collisions* (North-Holland, New York, 1970), Chap. 7, pp. 307–372.

[55] N. Stolterfoht, Dielectronic processes and electron correlation in energetic ion-atom collisions, Nucl. Instrum. Methods Phys. Res., Sect. B **53**, 477 (1991).

[56] H.-P. Hülskötter, W. E. Meyerhof, E. Dillard, and N. Guardala, Evidence for electron-electron interaction in projectile *K*-shell ionization, Phys. Rev. Lett. **63**, 1938 (1989).

[57] E. C. Montenegro, W. S. Melo, W. E. Meyerhof, and A. G. de Pinho, Separation of the screening and antiscreening effects in the electron loss of He^+ on H_2 and He, Phys. Rev. Lett. **69**, 3033 (1992).

[58] W. Wu, K. L. Wong, R. Ali, C. Y. Chen, C. L. Cocke, V. Frohne, J. P. Giese, M. Raphaelian, B. Walch, R. Dörner, V. Mergel, H. Schmidt-Böcking, and W. E. Meyerhof, Experimental separation of electron-electron and electron-nuclear contributions to ionization of fast hydrogenlike ions colliding with He, Phys. Rev. Lett. **72**, 3170 (1994).

[59] E. C. Montenegro and T. J. M. Zouros, On the relationship between the Born and the impulse approximations for the antiscreening process, Phys. Rev. A **50**, 3186 (1994).

[60] R. Dörner, V. Mergel, R. Ali, U. Buck, C. L. Cocke, K. Froschauer, O. Jagutzki, S. Lencinas, W. E. Meyerhof, S. Nüttgens, R. E. Olson, H. Schmidt-Böcking, L. Spielberger, K. Tökesi, J. Ullrich, M. Unverzagt, and W. Wu, Electron-electron interaction in projectile ionization investigated by high resolution recoil ion momentum spectroscopy, Phys. Rev. Lett. **72**, 3166 (1994).

[61] H. Kollmus, R. Moshammer, R. E. Olson, S. Hagmann, M. Schulz, and J. Ullrich, Simultaneous projectile-target ionization: A novel approach to $(e, 2e)$ experiments on ions, Phys. Rev. Lett. **88**, 103202 (2002).

[62] W. Mehlhorn and K. Taulbjerg, Angular distribution of electrons from autoionising states with unresolved fine structure, J. Phys. B **13**, 445 (1980).

[63] A. Müller, E. Lindroth, S. Bari, A. Borovik, P.-M. Hillenbrand, K. Holste, P. Indelicato, A. L. D. Kilcoyne, S. Klumpp, M. Martins, J. Viefhaus, P. Wilhelm, and S. Schippers, Photoionization of metastable heliumlike $C^{4+}(1s2s\,^3S_1)$ ions: Precision study of intermediate doubly excited states, Phys. Rev. A **98**, 033416 (2018).

[64] F. F. Goryaev, L. A. Vainshtein, and A. M. Urnov, Atomic data for doubly-excited states $2lnl'$ of He-like ions and $1s2lnl'$ of Li-like ions with $Z = 6 - 36$ and $n = 2, 3$, At. Data Nucl. Data Tables **113**, 117 (2017).

[65] S. Nanos, A. Biniskos, A. Laoutaris, M. Andrianis, T. J. M. Zouros, A. Lagoyannis, and E. P. Benis, Determination of the ion beam energy width in tandem Van de Graaff accelerators via Auger projectile spectroscopy, Nucl. Instrum. Methods Phys. Res., Sect. B **541**, 93 (2023).

[66] T. J. M. Zouros, S. Nikolaou, I. Madesis, A. Laoutaris, S. Nanos, A. Dubois, and E. P. Benis, Radiative cascade repopulation of $1s2s2p\,^4P$ states formed by single electron capture in 2–18 MeV collisions of $C^{4+}(1s2s\,^3S)$ with He, Atoms **8**, 61 (2020).

[67] M. Pajek and R. Schuch, X-rays from recombination of bare ions with electrons in an electron cooler, Nucl. Instrum. Methods Phys. Res., Sect. B **98**, 165 (1995).

[68] L. Natarajan, Fluorescence yields for doubly excited $2s3s$ configuration in He-like ions, Can. J. Phys. **97**, 382 (2019).

[69] D. H. Lee, T. J. M. Zouros, J. M. Sanders, P. Richard, J. M. Anthony, Y. D. Wang, and J. H. McGuire, *K*-shell ionization of O^{4+} and C^{2+} ions in fast collisions with H_2 and He gas targets, Phys. Rev. A **46**, 1374 (1992).

[70] E. C. Montenegro and W. E. Meyerhof, Passive and active electrons in the electron loss process, in *Two-Center Effects in Ion-Atom Collisions*, AIP Conference Proceedings, Vol. 362, edited by T. J. Gay and A. F. Starace, *American Institute of Physics* (AIP Press, New York, 1995), pp. 103–112.

[71] E. C. Montenegro, W. S. Melo, W. E. Meyerhof, and A. G. de Pinho, Intermediate-velocity atomic collisions. VI. Screening, antiscreening, and related processes in $He^+ + (H_2, He)$, Phys. Rev. A **48**, 4259 (1993).